ON THE PRACTICALITY OF DETERMINISTIC EPISTEMIC UNCERTAINTY

Anonymous authors
Paper under double-blind review

ABSTRACT

A set of novel approaches for estimating epistemic uncertainty in deep neural networks with a single forward pass has recently emerged as a valid alternative to Bayesian Neural Networks. On the premise of informative representations, these deterministic uncertainty methods (DUMs) achieve strong performance on detecting out-of-distribution (OOD) data while adding negligible computational costs at inference time. However, it remains unclear whether DUMs are well calibrated and can seamlessly scale to real-world applications - both prerequisites for their practical deployment. To this end, we first provide a taxonomy of DUMs, and evaluate their calibration under continuous distributional shifts. Then, we extend them to semantic segmentation. We find that, while DUMs scale to realistic vision tasks and perform well on OOD detection, the practicality of current methods is undermined by poor calibration under distributional shifts.

1 INTRODUCTION

Despite the dramatic enhancement of predictive performance of deep learning (DL), its adoption remains limited due to unpredictable failure on out-of-distribution (OOD) samples (1; 2) and adversarial attacks (3). Uncertainty estimation techniques aim at bridging this gap by providing accurate confidence levels on a model's output, allowing for a safe deployment of neural networks (NNs) in safety-critical tasks, *e.g.* autonomous driving or medical applications.

While Bayesian Neural Networks (BNNs) represent the predominant holistic solution for quantifying uncertainty (4; 5), exactly modelling their full posterior is often intractable, and scalable versions usually require expensive variational approximations (6; 7; 8; 9; 10). Moreover, it has recently been shown that true Bayes posterior can also lead to poor uncertainty (11). Thus, efficient approaches to uncertainty estimation largely remain an open problem, limiting the adoption within real-time applications under strict memory, time and safety requirements.

Recently, a promising line of work emerged estimating epistemic uncertainty in deterministic NNs with a single forward pass. By regularizing the hidden representations of a model, these methods represent an efficient and scalable solution to epistemic uncertainty estimation and to the related OOD detection problem. Compared to traditional uncertainty estimation techniques, Deterministic Uncertainty Methods (DUMs) quantify epistemic uncertainty by measuring distances (12; 13) or estimating the distribution of latent representations (14; 15; 16; 17; 18; 19; 20; 21). While OOD detection is a prerequisite for a safe deployment of DL in previously unseen scenarios, the calibration - *i.e.* how well uncertainty correlates with model performance - of such methods under continuous distributional shifts is equally important. Nonetheless, previous work falls short of investigating calibration, and solely focuses on OOD detection (12; 13; 16; 18; 19). Further, DUMs have thus far only been evaluated on toy datasets for binary classification, small-scale image classification tasks (13; 19) and toy prediction problems in natural language processing (15). Despite claiming to solve practical issues of traditional uncertainty estimation approaches, the practicality of DUMs remains to be assessed on more challenging tasks.

This work investigates the most crucial questions on the safety of DUMs in practical applications and addresses shortcomings and scalability issues. In particular: (i) we provide the first analysis of the calibration of DUMs under continuous distributional shifts; (ii) we evaluate the sensitivity of DUMs to their regularization strength; (iii) we scale DUMs to dense prediction tasks, *e.g.* semantic segmentation, and evaluate them under synthetic and realistic continuous distributional shift; (iv) we

find that the practicality of many DUMs is undermined by their poor calibration under both synthetic and realistic distributional shifts.

2 Related Work

Sources of Uncertainty. Uncertainty in a model's predictions can arise from two different sources (22; 23). While *aleatoric* uncertainty encompasses the noise inherent in the data and is consequently irreducible (22), *epistemic* uncertainty quantifies the uncertainty associated with choosing the model parameters based on limited information, and vanishes - in principle - in the limit of infinite data. This work distinguishes two properties of epistemic uncertainty - its performance on detecting OOD samples and its calibration (i.e. its correlation with model performance under distributional shifts). While the latter has been explored in the case of probabilistic approaches to uncertainty estimation (24) we are the first to investigate the behaviour of DUMs in this scenario. Notably, (25) evaluates prominent scalable epistemic uncertainty estimates on semantic segmentation. However, they investigate calibration only on in-distribution data. Further, although (15) evaluates the calibration of their approach, they do so exclusively on in-distribution data.

BNNs (26; 5) represent a principled way of measuring uncertainty. However, their intractable posterior distribution requires approximate inference methods, such as Markov Chain Monte-Carlo (26) or Variational Inference (VI) (4). While these methods traditionally struggle with large datasets and architectures, a variety of scalable approaches - often based on VI - have recently emerged.

Deep Ensembles, which typically consist of identical models trained from different initializations, have been introduced to the deep learning community by Lakshminarayanan *et al.* (27) and extended by (28; 29). While deep ensembles are widely regarded as a strong baseline for estimating epistemic uncertainty, they come with high computational as well as memory costs.

Efficient Approaches. Recently, a variety of approaches based on stochastic regularization have been developed (6; 7; 8; 30). By keeping stochasticity at inference time, they estimate uncertainty using multiple forward passes. Moreover, efficient ensemble methods were proposed producing predictions using a single model (31; 29; 28). Despite promising results on large-scale tasks while being parameter-efficient, these methods still require sampling through the model, which can render them impractical given limited compute. To estimate uncertainty in real-time and resource-demanding tasks, recent work has focused on providing uncertainty estimates with a *single forward pass*. One line of work proposes a principled approach for variance propagation in NNs (9; 32; 10).

Recently, DUMs showed promising results on OOD detection. By leveraging distances and densities in the feature space of a NN, these methods provide confidence estimates while adding negligible computational cost. Since they are united in their deterministic treatment of the weights, we term them Deterministic Uncertainty Methods (DUMs). The next section provides a taxonomy of DUMs.

3 Taxonomy for Deterministic Uncertainty Quantification

DUMs		**Uncertainty Estimation Method**			
		Discriminative		Generative	
		Distance from class centroid	Gaussian Processes	Gaussian Mixture Models	Normalizing Flows
Regu-larization	Distance awareness	DCS (12), DUQ (13)	SNGP (15), DUE (18)	DDU (19)	-
	Informative representations	-	-	DCU (16; 33), MIR (20)	Invertible networks (34; 35; 36)

Table 1: Taxonomy of DUMs. Methods are grouped according to their regularization of the hidden representations (rows), and their uncertainty estimation method (columns).

This section categorizes existing DUMs. To quantify epistemic uncertainty deterministically, the distribution of the hidden representations of a NN needs to be sensitive to the input distribution. However, discriminative models suffer from the fundamental problem of feature collapse (13; 19).

Thus, we firstly categorize DUMs according to the regularization method used to counteract feature collapse (Sec. 3.1). Moreover, we cluster DUMs according to the method used for uncertainty estimation (Sec. 3.2). Tab. 1 shows an overview of the resulting taxonomy.

Feature Collapse. Discriminative models can learn to discard large part of their input information, as exploiting spurious correlations may lead to better performance on the training data distribution (37; 38). Such invariant representations learned may be blind to distributional shifts, resulting in a collapse of OOD embeddings to in-distribution features This problem is known as *feature collapse* (13), and it makes OOD detection based on high-level representations impossible.

3.1 Regularization of Hidden Representations

We group DUMs according to how feature collapse is tackled. We identify two main paradigms - distance awareness and informative representations - which we discuss in Sec. 3.1.1 and Sec. 3.1.2.

3.1.1 Distance Awareness

Essentially, distance-aware hidden representations avoid feature collapse by relating distances between latent representations to distances in the input space. Therefore, one constrains the bi-Lipschitz constant, as it enforces a lower and an upper bound to expansion and contraction performed by a model. A lower bound enforces that different inputs are mapped to distinct representations and, thus, provides a solution to feature collapse. The upper bound enforces smoothness, *i.e.* small changes in the input do not result in large changes in the latent space. While there exist other approaches, *e.g.* (39), recent proposals have primarily adopted two methods to impose the bi-Lipschitz constraint.

The two-sided **Gradient Penalty** relates changes in the input to changes in feature space by directly constraining the gradient of the input (13). **Spectral Normalization (SN)** (40) is a less computationally-demanding alternative. SN is applicable to residual layers and normalizes the weights W of each layer using their spectral norm $sn(W)$ to constrain the bi-Lipschitz constant. Various DUMs - SNGP (15), DUE (18) and DDU (19) - rely on SN to enforce distance-awareness of hidden representations. More details on gradient penalty and SN can be found in the supplement.

Note that the Lipschitz constraint is defined with respect to a fix distance measure, which can be difficult to choose for many high-dimensional data distributions. A popular choice, e.g. (13; 15; 18), is the L_2 distance. Moreover, principled approaches to provide exact singular values in convolutional layers (41) result in prohibitive computational complexity; the spectral normalization approximations typically adopted by the methods previously described have been found to be sub-optimal (42), and its interaction with losses, architecture and optimization is yet to be fully understood (43).

3.1.2 Informative Representations

While methods enforcing distance-awareness achieve remarkable performance in OOD detection, they do not explicitly preserve sample-specific information. Consequently, depending on the underlying distance metric they may discard useful information about the input or act overly sensitive. An alternative line of work proposes to avoid feature collapse by learning informative representations (14; 16; 20; 35; 34; 36), thus forcing discriminative models to preserve information in its hidden representations beyond what is required to solve a task independent of the choice of an underlying distance metric. Notably, while representations that are aware of distances in the input space are also informative, both categories remain fundamentally different in their approach to feature collapse. While distance-awareness is based on the choice of a specific distance metric tying together input and latent space, informative representations incentivize a NN to store more information about the input using an auxiliary task (20; 16) or forbid information loss by construction (34; 35; 36). We identify three distinct families of approaches.

Contrastive learning (44) has emerged as an approach for learning representations that are both informative and discriminative. This is utilized by Wu *et al.* (16) and Winkens *et al.* (33), who apply SimCLR (45) to regularize hidden representations for a discriminative task by using a contrastive loss for pretraining and fine-tuning to force representations to discriminate between individual instances.

Reconstruction regularization (20) instead forces the intermediate activations to embody a complete representation of the input space. This is achieved by adding a decoder branch fed with the activations

of a given layer to reconstruct the input. Since this method aims at producing Maximally Informative Representations, we term it MIR.

Invertible Neural Networkss (INNs) (46; 34; 35; 36), built via a cascade of homeomorphic layers, cannot discard information except at the final classification stage. Consequently, the mutual information between input and hidden representation is maximized by construction. Interestingly, Behrmann *et al.* (47) showed that a ResNet is invertible if its Lipschitz constant is lower than 1, meaning that invertible ResNets both possess highly-informative representations and satisfy distance-awareness. However, note that this is not a necessary condition for invertibility, and thus information preservation.

3.2 Uncertainty Estimation

We distinguish two directions regarding uncertainty estimation in DUMs - generative and discriminative approaches. While generative approaches use the likelihood produced by an explicit generative model of the distribution of hidden representations as a proxy for uncertainty, discriminative methods directly use the predictions based on regularized representations to quantify uncertainty.

Generative approaches estimate the distribution of hidden representations post-training and use the likelihood as uncertainty metric to detect OOD samples. Wu *et al.* (16) propose a Deep Contrastive Uncertainty (DCU) method to train an additional deep network from the representation space to a distribution space, where the variance of the distribution is used as a confidence measure. MIR (20), DDU (19) and DCU (33) fit a class-conditional GMM to their regularized hidden representations and use the log-likelihood as an epistemic uncertainty proxy. A special instance of the generative approaches are INNs as they directly estimate the training data distribution. This allows using the likelihood of the input data as a proxy of uncertainty. While this idea is appealing, it can lead to training difficulties, imposes strong constraints on the underlying feature extractor and in some instances even remains susceptible to OOD data (48).

Discriminative approaches use the predictions based on regularized representations to directly assess confidence. Mandelbaum *et al.* (12) propose to use a Distance-based Confidence Score (DCS) to estimate local density at a point as the Euclidean distance in the embedded space between the point and its k nearest neighbors in the training set. Similarly, DUQ (13) builds on Radial Basis Function (RBF) networks (49) and propose a novel centroid updating scheme. Uncertainty is estimated as the distance between the model output and the closest centroid. DUMs adopting SN (15; 18), and thus preserving L_2 distances, typically fit Gaussian processes (GPs) with RBF kernels on top of the learned feature space, extending distance awareness to the output layer. In particular, SNGP (15) relies on a Laplace approximation of the GP based on the random Fourier feature (RFF) expansion of the GP posterior (50). DUE (18) leverages instead the inducing point approximation (51; 52), allowing to pick an arbitrarily large number of inducing points without overfitting (53). The uncertainty is then derived respectively as the Dempster-Shafer metric (15) or the softmax entropy (18).

4 Evaluation of Deterministic Epistemic Uncertainty

We measure the calibration of DUMs under continuous distributional shifts in two parts. Firstly, we evaluate DUMs on image classification using synthetic corruptions (Sec. 4.1.1). Then, we extend DUMs to a large-scale dense prediction task - semantic segmentation (Sec. 4.2) - where we evaluate their calibration on synthetic corruptions (Sec. 4.2.1) based on Cityscapes and on more realistic distributional shifts (Sec. 4.2.2) based on data collected in the simulation environment CARLA (54).

Baselines. We compare DUMs with two baselines for estimating epistemic uncertainty - Monte-Carlo (MC) dropout (7) and deep ensembles (27). Moreover, we report the softmax entropy of a vanilla NN as a simple baseline that only uses aleatoric uncertainty. We refer to the supplement for details on uncertainty estimation in our baselines. Note, that while MC dropout and deep ensembles are expected to predict reasonably calibrated uncertainty, their computational footprint greatly outweighs DUMs. However, the softmax entropy is expected to yield suboptimal calibration under distributional shifts since it quantifies aleatoric uncertainty while adding no computational overhead.

Methods. We evaluate DUQ (13), SNGP (15) and DDU (19) as representatives of methods that enforce distance-awareness, since these cover both techniques - SN and gradient penalty - and apply different techniques for uncertainty estimation. We exclude DUE (18) since it provides limited

additional insights when including SNGP. Moreover, we exclude DCS (12) since it only leads to a marginal improvement according to their own experiments, and since their contrastive loss only operates on class centroids and, thus, is not expected to lead to distance awareness within clusters. Furthermore, we evaluate MIR (20) and DCU (33) as representatives of methods enforcing informative representations. However, we do not scale DCU to semantic segmentation since constrastive pretraining based on SimCLR (45) is computationally too demanding due to large batch sizes. Further, we do not evaluate methods based on invertible neural networks (35; 36) since they 1) enforce strict constraints on the underlying architecture (*e.g.* fixed dimensionality of hidden representations) and often lead to training instabilities.

Calibration Metrics. Typical metrics for measuring calibration are Expected Calibration Error (ECE) (55) and Brier score (56). However, since most DUMs, except SNGP, do not provide uncertainty in form of a probabilistic forecast, we cannot rely on measuring the calibration of probabilities. Thus, we will exploit another desired property of uncertainty to quantify calibration, namely the ability to distinguish between correct and incorrect predictions. In fact, we can consider this property as a relaxed version of calibrated probabilities, since it is independent of the absolute value of uncertainty estimates and only relies on their ordering of predictions relative to each other. We assess the calibration of uncertainty estimates under distributional shifts using two metrics. Firstly, we report the *Area Under the Receiver Operating Characteristic (AUROC)* obtained when separating correct and incorrect predictions based on the corresponding uncertainty. Moreover, we introduce a new metric, *Relative Area Under the Lift Curve (rAULC)*, based on the Area Under the Lift Curve (AULC) (57). The AULC is obtained by ordering the predictions according to increasing uncertainty and plotting the performance (*e.g.* accuracy) of all samples with an uncertainty value smaller than a certain quantile of the uncertainty against the quantile itself.

Formally, given a set of uncertainty quantiles $q_i \in [0, 1]$, $i \in [1, ..., S]$, with some quantile step width $0 < s < 1$ and the function $F(q_i)$ which returns the accuracy of all samples with uncertainty $u < q_i$, the AULC is defined as $AULC = -1 + \sum_{i \in [1,...,S]} s \frac{F(q_i)}{F_R(q_i)}$. Here, $F_R(\cdot)$ refers to a baseline uncertainty estimate that corresponds to random guessing, and we subtract 1 to shift the performance of the random baseline to zero. Note, if an uncertainty estimate is anti-correlated with a models' performance, this score can also be negative. To alleviate a bias towards better performing models, we further compute the rAULC by dividing the AULC by the AULC of a hypothetical (optimal) uncertainty estimation that perfectly orders samples according to model performance. In classification we measure AUROC and rAULC on the image-level, in semantic segmentation on the pixel-level. In all experiments we set the quantile step width to $s = \frac{1}{N}$, where N is the number of predictions.

We compute AUROC and rAULC on continuous distributional shifts 1) across all severities of distributional shifts (including the clean testset) and 2) for each severity separately. We use the former method to establish a quantitative comparison among the methods and the latter to depict the calibration evolution qualitatively as a function of the distributional shift's severity.

4.1 Image Classification

Datasets. We train DUMs on CIFAR-10 and CIFAR-100 (58) and evaluate on the corrupted versions of their test set CIFAR10/100-C (59) (Sec. 4.1.1). These include 15 synthetic corruptions, each with 5 levels of severity. Moreover, we explore how sensitive the calibration of DUMs is to the choice of regularization strength on MNIST (60) and FashionMNIST (61)).

Models and optimization. Each method shares the same backbone architecture and uses a method-specific prediction head. When training on CIFAR-10/100, the backbone architecture is a ResNet-50 (62) For the experiments regarding hyperparameter sensitivity on MNIST and Fashion-MNIST, we employ a multilayer perceptron (MLP) as feature extractor with 3 hidden layers of 100 dimensions each and ReLU activation functions. Each DUM is associated with a particular hyperparameter for the regularization of its hidden representations. We choose the hyperparameter such that it minimizes the validation loss. All results are averaged over 5 independent runs. The corresponding standard deviation can be found in the supplement where not present in the main paper. We refer to the supplement for a detailed description on the optimization procedure and hyperparameter grid search for our baselines and each DUM.

Method	CIFAR10-C			CIFAR100-C		
	ACC	AUROC	rAULC	ACC	AUROC	rAULC
Softmax	0.882	0.782	0.708	0.610	0.762	0.596
MC Dropout (7)	0.885	**0.866**	0.829	0.615	0.818	**0.726**
Ensemble (27)	0.910	0.85 0	**0.833**	0.628	**0.824**	0.713
SNGP (15)	0.903	0.833	0.766	0.611	0.788	0.623
DDU (19)	0.884	0.673	0.441	0.609	0.635	0.339
MIR (20)	0.889	0.79	0.697	0.617	0.726	0.514
DUQ (13)	0.860	0.773	0.614	-	-	-
DCU (33)	**0.945**	0.794	0.706	**0.642**	0.750	0.558

Table 2: We compare Softmax, MC Dropout (7), Deep Ensembles, SNGP, DDU, MIR, DUQ and DCU on CIFAR10/100-C. We evaluate the accuracy (ACC) on the uncorrupted testset, AUROC and rAULC. Ensembles and MC dropout demonstrate better uncertainty calibration than most DUMs. Only SNGP consistently outperforms the softmax entropy. DCU's superior performance is expected since it uses expensive contrastive pretraining. DUQ did not converge on CIFAR100-C due to training instabilities arising from dynamically updated cluster centroids.

4.1.1 Continuous Distributional Shifts

Tab. 2 reports testset accuracy and calibration for the baselines and DUMs. AUROC and rAULC are computed for each corruption across all severity levels, then averaged over all corruptions. Further, Fig. 1 depicts our metrics depending on the severity of corruptions. We generally observe that ensembles and MC dropout demonstrate best performance in terms of calibration. Further, SNGP is the only DUM that consistently outperforms the softmax entropy. Overall we observe that DUMs using the distribution of hidden representations for estimating epistemic uncertainty yield worse calibration. Among these we find that regularizing hidden representations by enforcing distance awareness (DDU) yields the worst calibration. The superior performance of DCU (33) in terms of testset accuracy originates from their extensive contrastive pretraining which includes extensive data augmentation and a prolonged training schedule. We note that DUQ (13) did not converge on CIFAR100 due to training instabilities. These arise from maintaining the class centroids, which become very noisy for 100 classes with only 600 samples per class.

Moreover, we report OOD detection performance of models used in Tab. 2 and Fig. 1 in the supplement. Interestingly, despite competitive performance of OOD detection DUMs fall short in terms of uncertainty calibration compared to MC dropout and deep ensembles.

4.1.2 Sensitivity to Hyperparameters

We are interested in the qualitative impact of the regularization strength on the uncertainty calibration. Therefore, we train DUQ (13), SNGP (15), MIR (20) and DDU (19) using various regularization strengths on MNIST and evaluate on continuously shifted data by rotating from 0 to 180 degrees in steps of 20 degrees. Fig. 2 depicts the test accuracy against the rAULC for various regularization strengths. Only for MIR we observe a clear, positive correlation between regularization strength and calibration. The supplement depicts similar results on FashionMNIST (61).

4.2 Semantic Segmentation

This section evaluates whether DUMs seamlessly scale to realistic vision tasks and compares their behaviour under synthetic and realistic continuous distributional shifts with the softmax entropy, MC dropout and ensembles. Therefore, we apply MIR (20), SNGP (15) and DDU (19) to semantic segmentation. Note that DUQ (13) did not converge on this task.

We consider semantic segmentation as a multidimensional classification problem, where each pixel of the output mask represents an independent classification problem. Given an image $\mathbf{x}$ with n pixels $\mathbf{y} = \{y_1, \cdots, y_n\}$, the predictive distribution factorizes according to $p(\mathbf{y} \mid \mathbf{x}) = p(y_1 \mid \mathbf{x})p(y_2 \mid \mathbf{x}) \cdots p(y_n \mid \mathbf{x})$. We evaluate the calibration of the pixel-level uncertainty in our experiments.

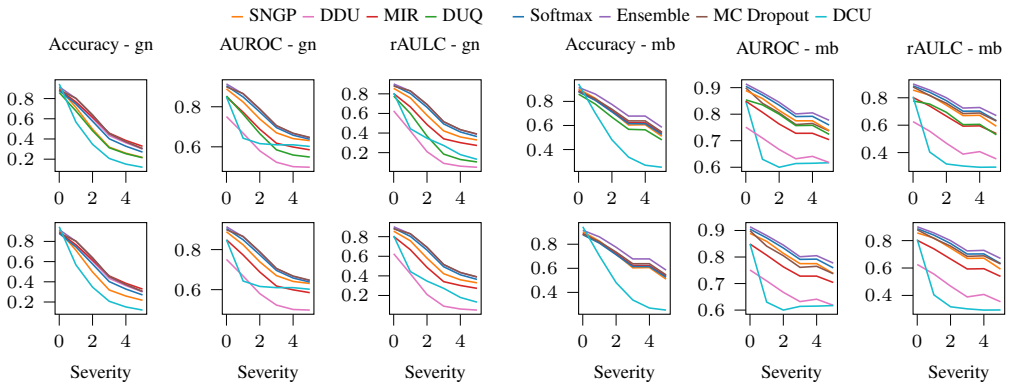

Figure 1: Softmax entropy, ensembles (27), MC dropout (7), DUQ (13), SNGP (15), MIR (20), DDU (19) and DCU (33) on CIFAR10-C (upper row) and CIFAR100-C (lower row) (59). We show the accuracy, AUROC and rAULC for each method on the corruptions gaussian_noise (gn) and motion_blur (mb) depending on the corruption severity. While all methods, except DCU, demonstrate a similar accuracy pattern, DUMs - in particular methods based on generative modeling of hidden representations - yield worse calibration across corruption severities. DUQ did not converge on CIFAR100. Other corruptions are included in the supplement.

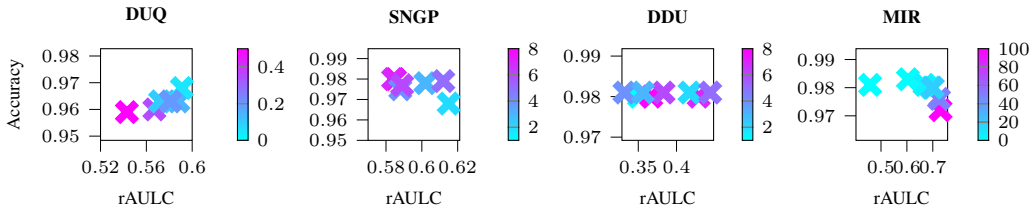

Figure 2: We analyse the sensitivity of DUQ (13), SNGP (15), MIR (20) and DDU (19) to their regularization strength. Therefore, we train models on MNIST and evaluate on continuously shifted data by rotating from 0 to 180 degrees in steps of 20 degrees. We plot the accuracy on the unperturbed testset against the rAULC computed using data from all levels of perturbation. Only for MIR we observe a clear, positive correlation between regularization strength and calibration. For DDU and SNGP, smaller regularization parameter denotes stronger regularization.

Datasets. We evaluate on synthetic distributional shifts using a corrupted version of Cityscapes (63) (Cityscapes-C (64)) which contains the same corruptions as CIFAR10/100-C. To further benchmark DUMs in a realistically and continuously changing environment, we collect a synthetic dataset for semantic segmentation. We use the CARLA Simulator (54) for rendering the images and segmentation masks. The classes definition is aligned with the CityScape dataset (63). Training data is collected from four towns in CARLA. We produce 32 sequences from each town. Vehicles and pedestrians are randomly generated for each sequence. Every sequence has 500 frames with a sampling rate of 10 FPS. We uniformly sample a validation set. We introduce continuous distributional shifts by varying the time-of-the-day and weather conditions (visual examples and details on data collection are in the supplment). The time-of-the-day is parameterized by the sun's altitude angle, where $90°$ means mid-day (training data) and the $0°$ means dust/dawn. We produce samples with altitude angles from $90°$ to $15°$ by steps of $5°$, and $15°$ to $-5°$, where the environment changes sharply, in $1°$ steps. In order to continuously change the weather conditions, we increase the magnitude of the rain in four steps (see supplement for visual examples). We refer to this dataset as CARLA-C.

Backbone. We adopt Dilated ResNet (DRN) (65; 66) as semantic segmentation backbone since it is based on residual connections allowing the use SN. DRN introduces dilated convolutions to ResNet, effectively increasing the receptive field without increasing the number of layers or parameters. This improves the spatial accuracy of DRN, achieving satisfactory results on CityScapes (63). We adopt the variant DRN-A-50. All results are averaged across 5 independent repetitions.

SNGP. DRN uses 1×1 convolutions at the last layer to map the latest feature map to the predicted segmentation mask. This works under the assumption that all pixels in the output mask are i.i.d. random variables. Following this intuition, we extend SNGP to semantic segmentation by fitting a $GP : \mathbb{R}^Z \to \mathbb{R}^C$ at pixel level that maps from the deep feature dimension z to the number of classes c. By keeping the GP kernel parameters shared across all pixels, we simulate a 1×1 convolutional GPs, *i.e.* $\sigma : (H_l \times W_l \times Z) \to (H_l \times W_l \times C)$, where σ convolves the GP, H_l and W_l are, respectively, feature map height and width at layer l, Z is the number of latent features and C is the number of output classes. For details about the GP we refer to (15) or the supplement.

MIR and DDU. To estimate uncertainty, MIR and DDU require fitting the distribution of hidden representations. We fit a Gaussian mixture model (GMM) with 20 components (*i.e.* number of classes) to each spatial location of the hidden representations using features extracted from the training data independently. This assumes that the distribution is translation invariant and factorizes along the spatial dimensions of the latent space which. Pixel-level uncertainties are then computed using bi-cubic interpolation following a similar procedure as (67) in this framework. We refer to the supplement for more details

4.2.1 Cityscapes Corrupted

We evaluate the softmax entropy, ensembles (27), MC dropout (7), SNGP (15), MIR (20), DDU (19) on Cityscapes-C (64). and Fig. 3 depict mean Intersection over Union (mIoU) and calibration performance in terms of AUROC and rAULC. We obtain similar results on more realistic distributional shifts. Ensembles and MC dropout yield the best calibration, while among DUMs only SNGP consistently ourperforms the softmax entropy.

Method	**Cityscapes-C**			**CARLA-C**		
	mIoU	AUROC	rAULC	mIoU	AUROC	rAULC
Softmax	0.503	0.815	0.737	0.422	0.854	0.818
MC Dropout (7)	0.506	**0.846**	**0.785**	0.410	0.843	0.730
Ensemble (27)	0.525	0.835	0.751	**0.428**	**0.863**	0.812
SNGP (15)	**0.519**	0.833	0.759	0.424	0.853	**0.813**
DDU (19)	0.505	0.731	0.542	0.408	0.467	-0.038
MIR (20)	0.504	0.729	0.564	0.412	0.744	0.619

Table 3: We compare semantic segmentation using Softmax, MC Dropout (7), Deep Ensembles, SNGP, DDU and MIR on Cityscapes-C and CARLA-C. We evaluate the mIoU on the uncorrupted testset and AUROC/rAULC across all levels of corruption. Again, ensembles and MC dropout yield better calibrated uncertainty than most DUMs. Most notably, only SNGP consistently outperforms the softmax entropy. DUMs using an explicit generative model of hidden representations to estimate uncertainty perform particular bad on realistic distributional shifts (CARLA-C).

4.2.2 Realistic Continuous Distributional Shifts

Similarly, we evaluate the softmax entropy, ensembles (27), MC dropout (7), SNGP (15), MIR (20), DDU (19) on CARLA-C. and Fig. 4 depict mIoU and calibration performance in terms of AUROC and rAULC. Ensembles yield the best calibration. Among DUMs only SNGP consistently ourperforms the softmax entropy which is in line with the results on image classification (Sec. 4.1.1).

5 Conclusion & Discussion

This work investigated the calibration under continuous distributional shifts of DUMs which recently showed good OOD detection performance and are interesting for practical applications in need of efficient uncertainty quantification. Overall, we observe that such uncertainty estimates are considerably worse calibrated than scalable Bayesian methods. We observe this on image classification (Sec. 4.1.1) as well as semantic segmentation (Sec. 4.2) and on synthetic as well as more realistic distributional shifts. SNGP (15) denotes the only DUM that consistently yields better calibrated uncertainties under continuous distributional shifts than the softmax entropy.

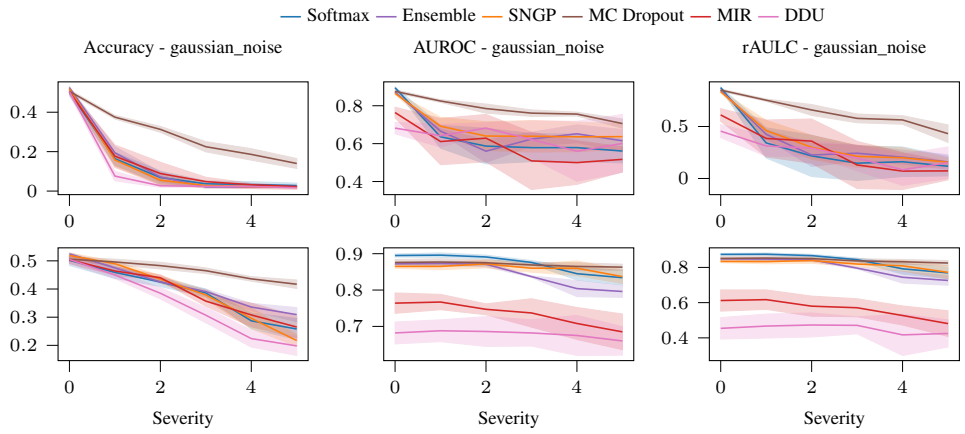

Figure 3: Softmax entropy, ensembles (27), MC dropout (7), SNGP (15), MIR (20), DDU (19) on Cityscapes-C (64). We show the mIoU, AUROC and rAULC for each method on the corruptions gaussian_noise (upper) and motion_blur (lower) depending on the corruption severity. While all methods demonstrate a similar mIoU pattern, DUMs - in particular methods based on generative modeling of hidden representations - yield worse calibration across corruption severities. Other corruptions are in the supplement.

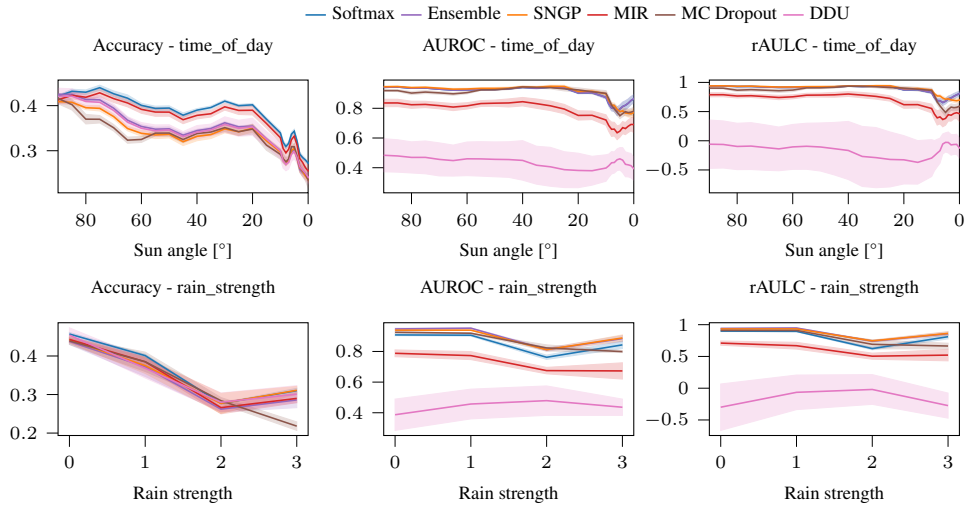

Figure 4: Softmax entropy, ensembles (27), MC dropout (7), SNGP (15), MIR (20), DDU (19) on CARLA-C (64). We show the mIoU, AUROC and rAULC for each method on the corruptions "time of day" (upper) and "rain" (lower) depending on the corruption severity. While all methods demonstrate a similar mIoU pattern, DUMs - in particular methods based on generative modeling of hidden representations - yield worse calibration across corruption severities.

In particular, our experiments reveal that methods relying on the distribution of hidden representations to quantify uncertainty (33; 20; 19) are poorly calibrated. Arguably, it is understandable that these methods are worse calibrated than SNGP since they do not take into account the predictive distribution. We refer to the supplement for a further theoretical consideration of the limitations of DUMs.

Moreover, another desirable property for such methods would be that the strength of the feature space regularization correlates with the quality of the uncertainty. However, this is not verified for Lipschitz regularization by our investigation (Sec. 4.1.1). We hypothesize that this originates from the choice of metric for regularization - *i.e.* L_2 distance - which is not meaningful in the image space. We hope that our findings will foster future research on making these promising family of methods better calibrated and more broadly applicable.

REFERENCES

[1] Gilles Blanchard, Gyemin Lee, and Clayton Scott. Generalizing from several related classification tasks to a new unlabeled sample. *Advances in neural information processing systems*, 24:2178–2186, 2011.

[2] Krikamol Muandet, David Balduzzi, and Bernhard Schölkopf. Domain generalization via invariant feature representation. In *International Conference on Machine Learning*, pages 10–18. PMLR, 2013.

[3] Christian Szegedy, Wojciech Zaremba, Ilya Sutskever, Joan Bruna, Dumitru Erhan, Ian Goodfellow, and Rob Fergus. Intriguing properties of neural networks. *arXiv preprint arXiv:1312.6199*, 2013.

[4] Geoffrey E Hinton and Drew Van Camp. Keeping the neural networks simple by minimizing the description length of the weights. In *Proceedings of the sixth annual conference on Computational learning theory*, pages 5–13, 1993.

[5] Radford M Neal. *Bayesian learning for neural networks*, volume 118. Springer Science & Business Media, 2012.

[6] Durk P Kingma, Tim Salimans, and Max Welling. Variational dropout and the local reparameterization trick. In *Advances in neural information processing systems*, pages 2575–2583, 2015.

[7] Yarin Gal and Zoubin Ghahramani. Dropout as a bayesian approximation: Representing model uncertainty in deep learning. In *international conference on machine learning*, pages 1050–1059, 2016.

[8] Guodong Zhang, Shengyang Sun, David Duvenaud, and Roger Grosse. Noisy natural gradient as variational inference. In *International Conference on Machine Learning*, pages 5852–5861. PMLR, 2018.

[9] Janis Postels, Francesco Ferroni, Huseyin Coskun, Nassir Navab, and Federico Tombari. Sampling-free epistemic uncertainty estimation using approximated variance propagation. In *Proceedings of the IEEE International Conference on Computer Vision*, pages 2931–2940, 2019.

[10] Antonio Loquercio, Mattia Segu, and Davide Scaramuzza. A general framework for uncertainty estimation in deep learning. *IEEE Robotics and Automation Letters*, 5(2):3153–3160, 2020.

[11] Florian Wenzel, Kevin Roth, Bastiaan Veeling, Jakub Swiatkowski, Linh Tran, Stephan Mandt, Jasper Snoek, Tim Salimans, Rodolphe Jenatton, and Sebastian Nowozin. How good is the bayes posterior in deep neural networks really? In *International Conference on Machine Learning*, pages 10248–10259. PMLR, 2020.

[12] Amit Mandelbaum and Daphna Weinshall. Distance-based confidence score for neural network classifiers. *arXiv preprint arXiv:1709.09844*, 2017.

[13] Joost Van Amersfoort, Lewis Smith, Yee Whye Teh, and Yarin Gal. Uncertainty estimation using a single deep deterministic neural network. In *International Conference on Machine Learning*, pages 9690–9700. PMLR, 2020.

[14] Alexander A Alemi, Ian Fischer, and Joshua V Dillon. Uncertainty in the variational information bottleneck. *arXiv preprint arXiv:1807.00906*, 2018.

[15] Jeremiah Zhe Liu, Zi Lin, Shreyas Padhy, Dustin Tran, Tania Bedrax-Weiss, and Balaji Lakshminarayanan. Simple and principled uncertainty estimation with deterministic deep learning via distance awareness. *Conference on Neural Information Processing Systems*, 2020.

[16] Mike Wu and Noah Goodman. A simple framework for uncertainty in contrastive learning. *arXiv preprint arXiv:2010.02038*, 2020.

[17] Bertrand Charpentier, Daniel Zügner, and Stephan Günnemann. Posterior network: Uncertainty estimation without ood samples via density-based pseudo-counts. *Advances in Neural Information Processing Systems*, 33:1356–1367, 2020.

[18] Joost van Amersfoort, Lewis Smith, Andrew Jesson, Oscar Key, and Yarin Gal. Improving deterministic uncertainty estimation in deep learning for classification and regression. *arXiv preprint arXiv:2102.11409*, 2021.

[19] Jishnu Mukhoti, Andreas Kirsch, Joost van Amersfoort, Philip HS Torr, and Yarin Gal. Deterministic neural networks with appropriate inductive biases capture epistemic and aleatoric uncertainty. *arXiv preprint arXiv:2102.11582*, 2021.

[20] Janis Postels, Hermann Blum, Yannick Strümpler, Cesar Cadena, Roland Siegwart, Luc Van Gool, and Federico Tombari. The hidden uncertainty in a neural networks activations. *arXiv preprint arXiv:2012.03082*, 2020.

[21] Bertrand Charpentier, Oliver Borchert, Daniel Zügner, Simon Geisler, and Stephan Günnemann. Natural posterior network: Deep bayesian predictive uncertainty for exponential family distributions. *arXiv preprint arXiv:2105.04471*, 2021.

[22] Armen Der Kiureghian and Ove Ditlevsen. Aleatory or epistemic? does it matter? *Structural safety*, 31(2):105–112, 2009.

[23] Alex Kendall and Yarin Gal. What uncertainties do we need in bayesian deep learning for computer vision? In *Proceedings of the 31st International Conference on Neural Information Processing Systems*, pages 5580–5590, 2017.

[24] Jasper Snoek, Yaniv Ovadia, Emily Fertig, Balaji Lakshminarayanan, Sebastian Nowozin, D Sculley, Joshua Dillon, Jie Ren, and Zachary Nado. Can you trust your model's uncertainty? evaluating predictive uncertainty under dataset shift. In *Advances in Neural Information Processing Systems*, pages 13969–13980, 2019.

[25] Fredrik K Gustafsson, Martin Danelljan, and Thomas B Schon. Evaluating scalable bayesian deep learning methods for robust computer vision. In *Proceedings of the IEEE/CVF Conference on Computer Vision and Pattern Recognition Workshops*, pages 318–319, 2020.

[26] Radford M Neal et al. Mcmc using hamiltonian dynamics. *Handbook of markov chain monte carlo*, 2(11):2, 2011.

[27] Balaji Lakshminarayanan, Alexander Pritzel, and Charles Blundell. Simple and scalable predictive uncertainty estimation using deep ensembles. In *Advances in neural information processing systems*, pages 6402–6413, 2017.

[28] Yeming Wen, Dustin Tran, and Jimmy Ba. Batchensemble: an alternative approach to efficient ensemble and lifelong learning. *arXiv preprint arXiv:2002.06715*, 2020.

[29] Michael Dusenberry, Ghassen Jerfel, Yeming Wen, Yian Ma, Jasper Snoek, Katherine Heller, Balaji Lakshminarayanan, and Dustin Tran. Efficient and scalable bayesian neural nets with rank-1 factors. In *International conference on machine learning*, pages 2782–2792. PMLR, 2020.

[30] Mattias Teye, Hossein Azizpour, and Kevin Smith. Bayesian uncertainty estimation for batch normalized deep networks. In *International Conference on Machine Learning*, pages 4907–4916, 2018.

[31] Christian Rupprecht, Iro Laina, Robert DiPietro, Maximilian Baust, Federico Tombari, Nassir Navab, and Gregory D Hager. Learning in an uncertain world: Representing ambiguity through multiple hypotheses. In *Proceedings of the IEEE International Conference on Computer Vision*, pages 3591–3600, 2017.

[32] Manuel Haußmann, Fred A Hamprecht, and Melih Kandemir. Sampling-free variational inference of bayesian neural networks by variance backpropagation. In *Uncertainty in Artificial Intelligence*, pages 563–573. PMLR, 2020.

[33] Jim Winkens, Rudy Bunel, Abhijit Guha Roy, Robert Stanforth, Vivek Natarajan, Joseph R Ledsam, Patricia MacWilliams, Pushmeet Kohli, Alan Karthikesalingam, Simon Kohl, et al. Contrastive training for improved out-of-distribution detection. *arXiv preprint arXiv:2007.05566*, 2020.

[34] Lynton Ardizzone, Jakob Kruse, Sebastian Wirkert, Daniel Rahner, Eric W Pellegrini, Ralf S Klessen, Lena Maier-Hein, Carsten Rother, and Ullrich Köthe. Analyzing inverse problems with invertible neural networks. *arXiv preprint arXiv:1808.04730*, 2018.

[35] Eric Nalisnick, Akihiro Matsukawa, Yee Whye Teh, Dilan Gorur, and Balaji Lakshminarayanan. Hybrid models with deep and invertible features. In *International Conference on Machine Learning*, pages 4723–4732. PMLR, 2019.

[36] Lynton Ardizzone, Radek Mackowiak, Carsten Rother, and Ullrich Köthe. Training normalizing flows with the information bottleneck for competitive generative classification. *Advances in Neural Information Processing Systems*, 33, 2020.

[37] Jonas Peters, Dominik Janzing, and Bernhard Schölkopf. *Elements of causal inference: foundations and learning algorithms*. The MIT Press, 2017.

[38] Mattia Segù, Alessio Tonioni, and Federico Tombari. Batch normalization embeddings for deep domain generalization. *arXiv preprint arXiv:2011.12672*, 2020.

[39] Anton Obukhov, Maxim Rakhuba, Alexander Liniger, Zhiwu Huang, Stamatios Georgoulis, Dengxin Dai, and Luc Van Gool. Spectral tensor train parameterization of deep learning layers. In *International Conference on Artificial Intelligence and Statistics*, pages 3547–3555. PMLR, 2021.

[40] Takeru Miyato, Toshiki Kataoka, Masanori Koyama, and Yuichi Yoshida. Spectral normalization for generative adversarial networks. *arXiv preprint arXiv:1802.05957*, 2018.

[41] Hanie Sedghi, Vineet Gupta, and Philip M Long. The singular values of convolutional layers. *arXiv preprint arXiv:1805.10408*, 2018.

[42] Sahil Singla and Soheil Feizi. Bounding singular values of convolution layers. *arXiv preprint arXiv:1911.10258*, 2019.

[43] Mihaela Rosca, Theophane Weber, Arthur Gretton, and Shakir Mohamed. A case for new neural network smoothness constraints. *arXiv preprint arXiv:2012.07969*, 2020.

[44] Aaron van den Oord, Yazhe Li, and Oriol Vinyals. Representation learning with contrastive predictive coding. *arXiv preprint arXiv:1807.03748*, 2018.

[45] Ting Chen, Simon Kornblith, Mohammad Norouzi, and Geoffrey Hinton. A simple framework for contrastive learning of visual representations. In *International conference on machine learning*, pages 1597–1607. PMLR, 2020.

[46] Jörn-Henrik Jacobsen, Arnold Smeulders, and Edouard Oyallon. i-revnet: Deep invertible networks. *arXiv preprint arXiv:1802.07088*, 2018.

[47] J Behrmann, W Grathwohl, RTQ Chen, D Duvenaud, and JH Jacobsen. Invertible residual networks. arxiv e-prints. *arXiv preprint arXiv:1811.00995*, 2018.

[48] Eric Nalisnick, Akihiro Matsukawa, Yee Whye Teh, Dilan Gorur, and Balaji Lakshminarayanan. Do deep generative models know what they don't know? In *International Conference on Learning Representations*, 2018.

[49] Yann LeCun, Léon Bottou, Yoshua Bengio, and Patrick Haffner. Gradient-based learning applied to document recognition. *Proceedings of the IEEE*, 86(11):2278–2324, 1998.

[50] Carl Edward Rasmussen. Gaussian processes in machine learning. In *Summer school on machine learning*, pages 63–71. Springer, 2003.

[51] Michalis Titsias. Variational learning of inducing variables in sparse gaussian processes. In *Artificial intelligence and statistics*, pages 567–574. PMLR, 2009.

[52] James Hensman, Alexander Matthews, and Zoubin Ghahramani. Scalable variational gaussian process classification. In *Artificial Intelligence and Statistics*, pages 351–360. PMLR, 2015.

[53] David Burt, Carl Edward Rasmussen, and Mark Van Der Wilk. Rates of convergence for sparse variational gaussian process regression. In *International Conference on Machine Learning*, pages 862–871. PMLR, 2019.

[54] Alexey Dosovitskiy, German Ros, Felipe Codevilla, Antonio Lopez, and Vladlen Koltun. CARLA: An open urban driving simulator. In *Proceedings of the 1st Annual Conference on Robot Learning*, pages 1–16, 2017.

[55] Mahdi Pakdaman Naeini, Gregory Cooper, and Milos Hauskrecht. Obtaining well calibrated probabilities using bayesian binning. In *Proceedings of the AAAI Conference on Artificial Intelligence*, volume 29, 2015.

[56] GLENN W BRIER. Verification of forecasts expressed in terms of probability. *Monthly Weather Review*, 78(1):1–3, 1950.

[57] Miha Vuk and Tomaz Curk. Roc curve, lift chart and calibration plot. *Metodoloski zvezki*, 3(1):89, 2006.

[58] Alex Krizhevsky, Vinod Nair, and Geoffrey Hinton. The cifar-10 dataset. *online: http://www. cs. toronto. edu/kriz/cifar. html*, 55:5, 2014.

[59] Dan Hendrycks and Thomas Dietterich. Benchmarking neural network robustness to common corruptions and perturbations. *Proceedings of the International Conference on Learning Representations*, 2019.

[60] Yann LeCun. The mnist database of handwritten digits. *http://yann. lecun. com/exdb/mnist/*, 1998.

[61] Han Xiao, Kashif Rasul, and Roland Vollgraf. Fashion-mnist: a novel image dataset for benchmarking machine learning algorithms. *arXiv preprint arXiv:1708.07747*, 2017.

[62] Kaiming He, Xiangyu Zhang, Shaoqing Ren, and Jian Sun. Deep residual learning for image recognition. In *Proceedings of the IEEE conference on computer vision and pattern recognition*, pages 770–778, 2016.

[63] Marius Cordts, Mohamed Omran, Sebastian Ramos, Timo Rehfeld, Markus Enzweiler, Rodrigo Benenson, Uwe Franke, Stefan Roth, and Bernt Schiele. The cityscapes dataset for semantic urban scene understanding. In *Proc. of the IEEE Conference on Computer Vision and Pattern Recognition (CVPR)*, 2016.

[64] Claudio Michaelis, Benjamin Mitzkus, Robert Geirhos, Evgenia Rusak, Oliver Bringmann, Alexander S Ecker, Matthias Bethge, and Wieland Brendel. Benchmarking robustness in object detection: Autonomous driving when winter is coming. *arXiv preprint arXiv:1907.07484*, 2019.

[65] Fisher Yu and Vladlen Koltun. Multi-scale context aggregation by dilated convolutions. In *International Conference on Learning Representations (ICLR)*, 2016.

[66] Fisher Yu, Vladlen Koltun, and Thomas Funkhouser. Dilated residual networks. In *Computer Vision and Pattern Recognition (CVPR)*, 2017.

[67] Hermann Blum, Paul-Edouard Sarlin, Juan Nieto, Roland Siegwart, and Cesar Cadena. The fishyscapes benchmark: Measuring blind spots in semantic segmentation. *arXiv preprint arXiv:1904.03215*, 2019.